PHYSICAL REVIEW B, VOLUME 64, 020401(R)

Magnetic structure of heavy-fermion Ce_2RhIn_8

Wei Bao, P. G. Pagliuso, J. L. Sarrao, J. D. Thompson, and Z. Fisk*
Los Alamos National Laboratory, Los Alamos, New Mexico 87545

J. W. Lynn
NIST Center for Neutron Research, National Institute of Standards and Technology, Gaithersburg, Maryland 20899

(Received 12 February 2001; published 7 June 2001)

The magnetic structure of the heavy-fermion antiferromagnet Ce_2RhIn_8 is determined using neutron diffraction. It is a collinear antiferromagnet with a magnetic wave vector (1/2,1/2,0) and a staggered moment of $0.55(6)\mu_B$ per Ce at 1.6 K, tilted 38(2)° from the tetragonal c axis. In spite of its layered crystal structure, the phases for the magnetic moments are the same as those in the cubic parent antiferromagnet $CeIn_3$. This suggests that the cubic $CeIn_3$ building blocks have a stronger influence on magnetic correlations than intervening $RhIn_2$ layers, which give the material its apparent two-dimensional lattice structure and renders $CeRhIn_5$ an incommensurate antiferromagnet.

DOI: 10.1103/PhysRevB.64.020401 PACS number(s): 75.25.+z, 75.30.Mb, 71.27.+a

Superconducting heavy-fermion materials belong to a special class of correlated electron systems where unconventional superconductivity is believed to be mediated by antiferromagnetic fluctuations.[1] Until recently, there were only five U-based heavy fermion materials showing superconductivity at ambient pressure[2] in addition to the original heavy-fermion superconductor $CeCu_2Si_2$.[3] Three Ce-based heavy-fermion materials isostructural to $CeCu_2Si_2$ and cubic $CeIn_3$ become superconductors under pressure.[4–6] Recently, superconductivity has been discovered in a new structure class of heavy-fermion materials with chemical formula $CeMIn_5$. The Sommerfeld constants $\gamma\approx0.4$, 0.7, and 0.3 J/mole K^2 for $M=$Rh, Ir, and Co, respectively.[7–9] While the $M=$Rh member superconducts below 2.1 K under pressures above 17 kbar,[7] the $M=$Ir and Co members superconduct below 0.4 K and 2.3 K, respectively, at ambient pressure.[8,9] The high superconducting transition temperatures of the new materials hold the record for heavy-fermion superconductors. Thermodynamic and transport measurements at low temperature are consistent with unconventional superconductivity in which there are lines of nodes in the superconducting gap.[10]

Because $CeIn_3$ and $CeMIn_5$ belong to the $Ce_nM_mIn_{3n+2m}$ family of structures, they present a unique opportunity for investigating the influence of systematic structure modifications on the superconducting and magnetic properties.[11] In particular, it is interesting to compare $CeIn_3$ and $CeRhIn_5$, which are the $n=\infty$ and $n=1$ members of the Ce_nRhIn_{3n+2} subfamily, and can be viewed as periodic stacking of n layers of $CeIn_3$ on a layer of MIn_2.[12,13] Both are antiferromagnetic at ambient pressure with $T_N=10$ K for $CeIn_3$ (Ref. 14) and $T_N=3.8$ K for $CeRhIn_5$.[7,15] Both become superconductors when subjected to pressure, with the superconducting transition temperature of $CeRhIn_5$ being one order of magnitude higher than that for $CeIn_3$ [$T_C=0.25$ K at 25 kbar (Ref. 6)]. This raises a fundamental question about the role of the intervening MIn_2 layers on both the superconductivity and antiferromagnetism. Our study of Ce_2RhIn_8, which is the $n=2$ member of this heavy-fermion subfamily, is intended to shed light on this question by changing the ratio of the $CeIn_3$ and $RhIn_2$ layers.

Antiferromagnetic structures for both $CeIn_3$ and $CeRhIn_5$ have been determined previously using neutron diffraction. Cubic $CeIn_3$ has a simple commensurate magnetic order with wave vector (1/2,1/2,1/2) below its Néel temperature[16,17] (refer to Fig. 1). The staggered magnetic moment is $0.48\mu_B$–$0.65\mu_B$ per Ce, and the moment direction cannot be determined by neutron diffraction for this cubic system.[16,17] In contrast, magnetic moments of Ce ions in tetragonal $CeRhIn_5$ form an incommensurate transverse spiral below $T_N=3.8$ K, with wave vector (1/2,1/2,0.297) (Ref. 18) (refer to Fig. 1). The staggered moment of $0.37\mu_B$ per Ce at 1.4 K is smaller than that for $CeIn_3$. In this paper, we report the magnetic structure for Ce_2RhIn_8, which orders at $T_N=2.8$ K.[11] The commensurate antiferromagnetic structure for this $n=2$ material (refer to Fig. 1) closely resembles that for $CeIn_3$ ($n=\infty$), rather than the magnetic spiral of $CeRhIn_5$ ($n=1$). This suggests a strong influence of the cubic $CeIn_3$ structural unit on magnetic correlations in this family of heavy-fermion materials.

Single crystals of Ce_2RhIn_8 were grown from an In flux. They crystallize in the tetragonal Ho_2CoGa_8 structure (space group No. 123, $P4/mmm$),[12] with lattice parameters $a=4.665$ Å and $c=12.244$ Å at room temperature. The inverse static magnetic susceptibility, measured with a superconducting quantum interference device magnetometer with a 1 kOe field parallel (circles) and perpendicular (squares) to the c axis, is shown in Fig. 2. The high-temperature effective moment, from data above 200 K, shows only small anisotropy, with 2.38 μ_B and 2.32 μ_B per Ce for magnetic field parallel and perpendicular to the c axis, respectively. They are slightly reduced from the Hund's rule value of 2.54 μ_B. The Curie-Weiss temperatures have different signs, $+12$ K for a field along the c axis and -40 K for a field perpendicular to the c axis, which is not uncommon for rare-earth magnets.[19] There is no cusp in χ at the Néel temperature. The Sommerfeld constant, $\gamma\approx0.4$ J/mole Ce K^2, qualifies Ce_2RhIn_8 as a heavy-fermion compound.[11]

The sample used in this study was a well-faceted rectangular plate of dimension $\sim4\times4\times0.7$ mm and weight of 88

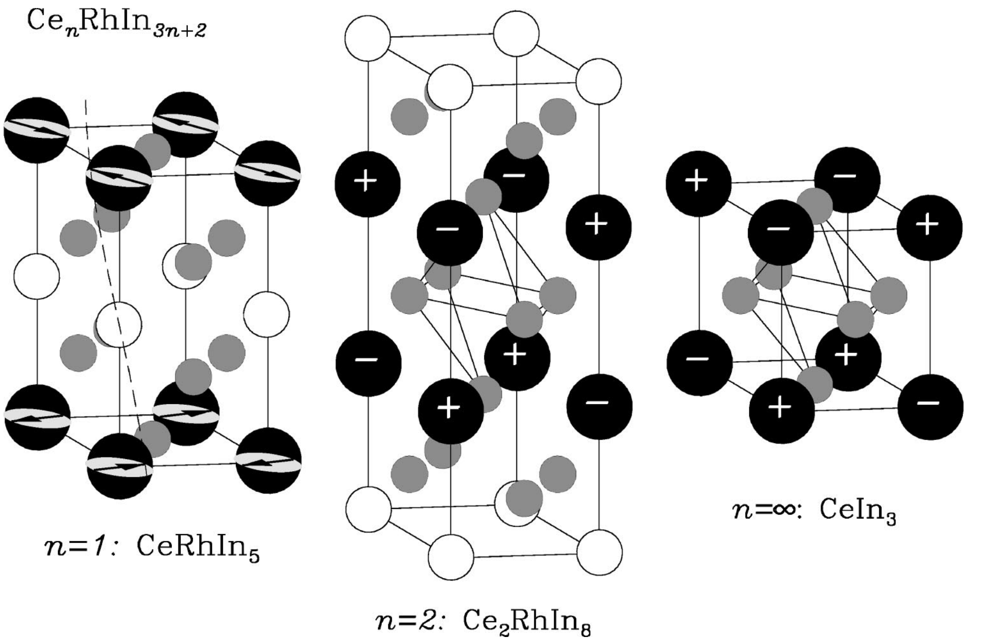

FIG. 1. The magnetic structure of Ce_2RhIn_8 ($n=2$) in a structural unit cell is shown together with $CeRhIn_5$ ($n=1$) and $CeIn_3$ ($n=\infty$). The solid circle denotes Ce, the shaded circle In, and the open circle Rh. The magnetic moment is $0.55\mu_B$ per Ce in Ce_2RhIn_8 and it points 38° from the c axis. The magnetic moment, $0.37\mu_B$ per Ce, in $CeRhIn_5$ forms an incommensurate spiral (Refs. 18 and 15). The disk denotes the plane in which the ordered moment rotates. The magnetic moment is $0.48\mu_B$–$0.65\mu_B$ per Ce in $CeIn_3$ and the moment direction has not been determined (Refs. 16 and 17).

mg. The largest surface is the (001) plane. Neutron diffraction experiments were performed at NIST using the thermal triple-axis spectrometer BT2 in a two-axis mode. The horizontal collimations were 60-40-40-open. Neutrons with incident energy $E=35$ meV were selected using the (002) reflection of a pyrolytic graphite (PG) monochromator. The neutron penetration length at this energy is 1.8 mm, which is substantially longer than the thickness of the sample. No rocking-angle-dependent absorption was noticed. PG filters of total 9 cm thickness were used to remove higher-order neutrons. The sample temperature was regulated by a top loading pumped He cryostat.

Temperature-dependent magnetic Bragg peaks were found at $(m/2,n/2,l)$ with m and n odd integers and l *nonzero* integers. This corresponds to a magnetic unit cell that doubles the structural unit cell in the basal plane and contains four magnetic Ce ions. Rocking scans at (1/2,1/2,0) and $(1/2,1/2,\overline{1})$, taken at 1.6 K, are shown in Fig. 3(a). The intensity of the (1/2,1/2,1) peak is shown in Fig. 3(b) as the square of the order parameter of the magnetic phase transition. Integrated intensities of magnetic Bragg peaks from such rocking scans are normalized to structural Bragg peaks (001), (002), (003), (005), (006), and (220) to yield magnetic scattering cross sections, $\sigma(\mathbf{q})=I(\mathbf{q})\sin(\theta_4)$, in absolute units (see Table I). In such units, the magnetic cross section is[20]

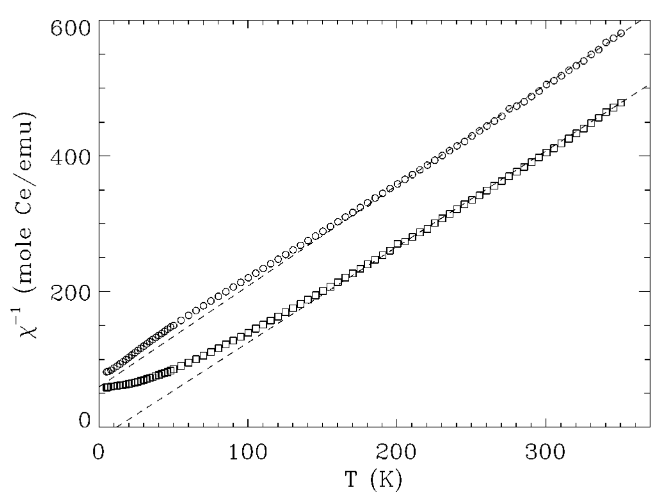

FIG. 2. Inverse magnetic susceptibility measured in an applied field of 1 kOe for the field along the c axis (circles) and perpendicular to the c axis (squares) of Ce_2RhIn_8. The dashed lines are fits to the Curie-Weiss law for data above 200 K.

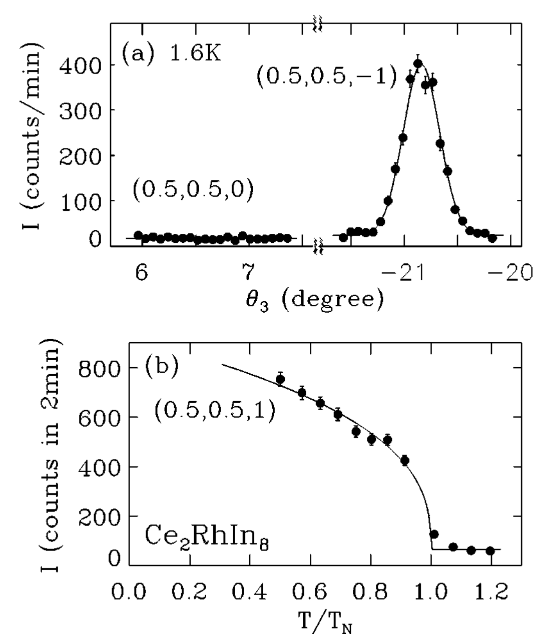

FIG. 3. (a) Elastic rocking scans through magnetic Bragg points (1/2,1/2,0) and (1/2,1/2,−1) at 1.6 K. The (1/2,1/2,0) is forbidden for this magnetic structure. (b) Intensity of (1/2,1/2,1) as a function of T/T_N. The Néel temperature is 2.8 K. The solid line is a guide to the eyes.

TABLE I. Magnetic Bragg intensity, σ_{obs}, defined in Eq. (1), observed at 1.6 K in units of 10^{-3} b per Ce_2RhIn_8. The theoretical intensity, σ_{cal}, is calculated using Eqs. (2) and (3) with $\beta=52°$ and $M=0.55\mu_B$/Ce. The resultant reliability coefficient $R=\Sigma|\sigma_{obs}-\sigma_{cal}|/\Sigma\sigma_{obs}$ is 8.9%.

q	σ_{obs}	σ_{cal}
(0.5 0.5 −1)	52(1)	46.2
(0.5 0.5 0)	0.0(3)	0.0
(0.5 0.5 1)	49(1)	46.2
(0.5 0.5 2)	19(1)	18.9
(0.5 0.5 3)	6.4(4)	5.5
(0.5 0.5 4)	21(1)	23.2
(0.5 0.5 6)	7.5(7)	7.6
(1.5 1.5 0)	0.0(8)	0.0
(1.5 1.5 1)	18(1)	24.8

$$\sigma(\mathbf{q})=\left(\frac{\gamma r_0}{2}\right)^2\langle M\rangle^2|f(q)|^2\sum_{\mu,\nu}(\delta_{\mu\nu}-\hat{q}_\mu\hat{q}_\nu)\mathcal{F}_\mu^*(\mathbf{q})\mathcal{F}_\nu(\mathbf{q}), \quad (1)$$

where $(\gamma r_0/2)^2=0.07265$ b/μ_B^2, M is the staggered moment of the Ce ion, $f(q)$ the Ce^{3+} magnetic form factor,[21] $\hat{\mathbf{q}}$ the unit vector of $\mathbf{q}$, and $\mathcal{F}_\mu(\mathbf{q})$ the μth Cartesian component of magnetic structure factor per Ce_2RhIn_8.

Forbidden peaks at $(m/2,m/2,0)$ provide an important clue to the magnetic structure of Ce_2RhIn_8. They could be due to magnetic moments aligning along the [110] direction. However, magnetic twinning in this tetragonal material will yield finite intensities at these reciprocal points. Another, more reasonable, cause is that the nearest-neighbor magnetic moments along the c axis are antiparallel. The phase between the next-nearest-neighbor magnetic moments along the c axis and the phases of magnetic moments in a basal layer are already determined by the magnetic wave vector. This yields a collinear antiferromagnetic structure as shown in Fig. 1 with magnetic cross sections per Ce_2RhIn_8

$$\sigma(\mathbf{q})=4\left(\frac{\gamma r_0}{2}\right)^2\langle M\rangle^2|f(q)|^2\langle 1-(\hat{\mathbf{q}}\cdot\hat{\mathbf{s}})^2\rangle\sin^2(l\epsilon), \quad (2)$$

where $2\epsilon=0.38c$ is the separation between the nearest-neighbor Ce ions along the c axis, $\hat{\mathbf{s}}$ is the unit vector of the magnetic moment, and the average, $\langle 1-(\hat{\mathbf{q}}\cdot\hat{\mathbf{s}})^2\rangle$, is over magnetic domains.

Figure 4 shows $\sigma_{obs}(\mathbf{q})/|f(q)|^2\sim\langle 1-(\hat{\mathbf{q}}\cdot\hat{\mathbf{s}})^2\rangle\sin^2(l\epsilon)$ as a function of the l index of $\mathbf{q}$. The structure factor, $4\sin^2(l\epsilon)$, not only accounts for the forbidden $l=0$ magnetic peaks, but it also accounts for the strong oscillation of σ_{obs} as a function of l. The remaining, smooth l dependence is to be accounted for by the polarization factor $\langle 1-(\hat{\mathbf{q}}\cdot\hat{\mathbf{s}})^2\rangle$.

For an arbitrary moment orientation, there are in general 16 magnetic M domains with tetragonal symmetry of Ce_2RhIn_8. The moment direction in the basal plane cannot be distinguished in the diffraction due to square symmetry.[22] However, moment direction relative to the c axis is determinable. Denote the angle between $\mathbf{q}$ and the basal plane as α, and the angle between the basal plane and the magnetic moment as β. Assuming equal populations among the M domains, we have

$$\langle 1-(\hat{\mathbf{q}}\cdot\hat{\mathbf{s}})^2\rangle=1-\frac{\cos^2\alpha\,\cos^2\beta+2\,\sin^2\alpha\,\sin^2\beta}{2}. \quad (3)$$

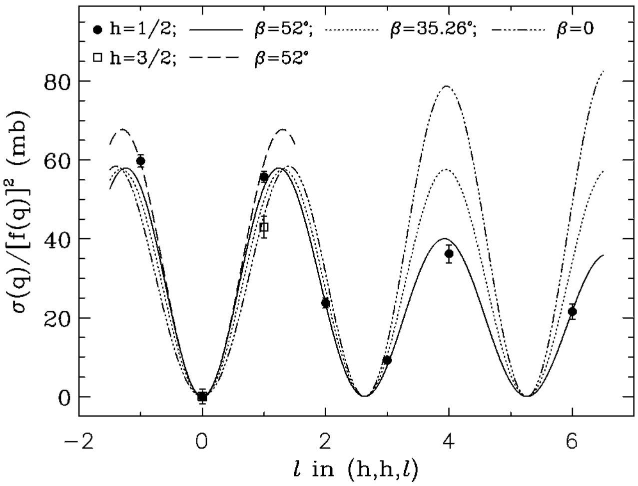

FIG. 4. The l dependence of the magnetic cross section, σ, divided by the form factor $|f(q)|^2$. The theoretical curves are calculated using Eqs. (2) and (3) with $M=0.55\mu_B$ and various values specified in the figure for the moment tilt angle, β.

For a magnetic moment lying in the basal plane, $\beta=0$, which is the case for $CeRhIn_5$,[18,15] the polarization factor varies too much and the resulting theoretical curve does not fit the data (refer to the dot-dashed line in Fig. 4). For $\beta=35.26°$, which corresponds to $\mathbf{s}$ in the $\langle 111\rangle$ directions in a cubic system, the polarization factor averages to a constant, 2/3. The resulting theoretical curve is a better fit (refer to the dotted line in Fig. 4) than that for $\beta=0$, but it is still not satisfactory. The best least-squares fit (refer to the solid and dashed lines for $h=k=1/2$ and $h=k=3/2$, respectively) yields $\beta=52(2)°$, with the reliability coefficient $R=\Sigma|\sigma_{obs}-\sigma_{cal}|/\Sigma\sigma_{obs}$ being 8.9%. The staggered magnetic moment is determined at 1.6 K to be $M=0.55(6)\mu_B$ per Ce.

Having determined the magnetic structure of Ce_2RhIn_8, we now consider the systematics relating the magnetic structure and lattice structure in Ce_nRhIn_{3n+2} (see Fig. 1 and Table II). In the a-b plane, the magnetic moments of the Ce ions form a square lattice, surrounded by In ions, in all three materials. They all are simple, nearest-neighbor antiferromagnets in the plane. In $CeRhIn_5$, this Ce antiferromagnetic plane alternates with the $RhIn_2$ layer. Magnetic correlations across the $RhIn_2$ layer are incommensurate, with neighboring magnetic moments being rotated by 107°.[18] The local structure environment in the vertical a-c or the b-c plane within the $CeIn_3$ double layer in Ce_2RhIn_8 is very similar to that in the basal layer. The same nearest-neighbor antiferromagnetic correlations exist in the double layers. It is interesting that now across the $RhIn_2$ layer the Ce moments are antiparallel instead of rotated by 107°. The insertion of the $RhIn_2$ layers between $CeIn_3$ bilayers, thus, does not modify the magnetic order relative to cubic $CeIn_3$. This suggests $CeRhIn_5$ as a

TABLE II. Physical properties of Ce_nRhIn_{3n+2}. Units for the Sommerfeld constant, γ, is mJ/K^2 mol; for the Néel temperature, T_N, and superconducting transition temperature, T_C, are K; for staggered moment, M, μ_B/Ce; for the critical pressure, P_C, of superconducting transition, kbar. γ for $CeIn_3$ is from Ref. 23. Refer to text for references for other quantities.

	n	γ	T_N	$\mathbf{q}_M$	M	T_C	P_C
$CeRhIn_5$	1	400	3.8	$(\frac{1}{2},\frac{1}{2},0.297)$	0.37	2.1	17
Ce_2RhIn_8	2	400	2.8	$(\frac{1}{2},\frac{1}{2},0)$	0.55	–	–
$CeIn_3$	∞	120	10.1	$(\frac{1}{2},\frac{1}{2},\frac{1}{2})$	0.48,0.65	0.25	25

unique member of the Ce_nRhIn_{3n+2} family, and the $n \geqslant 2$ members are likely to be magnetically similar to cubic $CeIn_3$. Searching for heavy-fermion materials with two-dimensional magnetism seems more profitable if one could find a CeM_mIn_{3+2m} structure family, where m MIn_2 layers separate a single $CeIn_3$ layer.

Another interesting difference between the $n=1$ and the $n=2$ materials concerns the magnetic moment orientation. In $CeRhIn_5$, the moments rotate in the *a-b* plane, indicating a *XY*-type magnetic anisotropy. In Ce_2RhIn_8, the magnetic moments point 52° from the basal plane. Different local anisotropic fields, together with crystal fields and isotropic exchange, likely contribute to the different magnetic structures in the two materials.[19] We also notice that the staggered moment of Ce_2RhIn_8 ($n=2$) is comparable to that of $CeIn_3$ ($n=\infty$), while T_N is quite different for them. In fact, $T_N/\langle M\rangle^2$ is the smallest for Ce_2RhIn_8 in the group. It will be interesting to see whether this is due to frustrating effect of the $RhIn_2$ layers which renders $CeRhIn_5$ incommensurate. Antiferromagnetic transitions have been studied in isostructural Nd_nMIn_{3n+2} ($M=$Rh,Ir and $n=1,2$) and crystal-field effects have been emphasized.[24] A detailed understanding of the magnetic interactions in these materials is essential in pursuing the magnetic origin of unconventional superconductivity in heavy-fermion Ce_nMIn_{3n+2}.

In summary, we find the magnetic structure of Ce_2RhIn_8 to be closely related to that of cubic $CeIn_3$. The staggered moment is $0.55(6)\mu_B$ per Ce at 1.6 K and it points 52° from the *a-b* plane. It is hoped that the determination of magnetic structures for the family Ce_nRhIn_{3n+2} ($n=1$, 2, and ∞) will allow theoretical magnetic models to be constructed, which is an essential component of understanding unconventional superconductivity in Ce_nMIn_{3n+2} ($n=1,\infty$; $M=$Rh, Ir, Co).

We thank M.E. Zhitomirsky and M.F. Hundley for useful discussions. W.B. thanks D.C. Dender for technical assistance at NIST. Work at Los Alamos was performed under the auspices of the U.S. Department of Energy. Z.F. gratefully acknowledges NSF support at FSU. P.G.P. also acknowledges FAPESP-SP (Brazil).

[*] Permanent address: Florida State University, Tallahassee, FL 32306.

[1] H. R. Ott and Z. Fisk, in *Handbook on the Physics and Chemistry of Actinides*, edited by A. J. Freeman and G. H. Lander (North-Holland, Amsterdam, 1987).

[2] R. H. Heffner and M. R. Norman, Comments Condens. Matter Phys. **17**, 361 (1996).

[3] F. Steglich, J. Aarts, C. D. Bredl, W. Lieke, D. Meschede, W. Franz, and H. Schäfer, Phys. Rev. Lett. **43**, 1892 (1979).

[4] D. Jaccard, K. Behnia, and J. Sierro, Phys. Lett. A **163**, 475 (1992).

[5] R. Movshovich *et al.*, Phys. Rev. B **53**, 8241 (1996).

[6] N. D. Mathur, F. M. Grosche, S. R. Julian, I. R. Walker, D. M. Freye, R. K. W. Haselwimmer, and G. G. Lonzarich, Nature (London) **394**, 39 (1998).

[7] H. Hegger, C. Petrovic, E. G. Moshopoulou, M. F. Hundley, J. L. Sarrao, Z. Fisk, and J. D. Thompson, Phys. Rev. Lett. **84**, 4986 (2000).

[8] C. Petrovic, R. Movshovich, M. Jaime, P. G. Pagliuso, M. F. Hundley, J. L. Sarrao, Z. Fisk, and J. D. Thompson, Europhys. Lett. **53**, 354 (2001).

[9] C. Petrovic, P. G. Pagliuso, M. F. Hundley, R. Movshovich, J. L. Sarrao, J. D. Thompson, Z. Fisk, and P. Monthoux, J. Phys.: Condens. Matter **13**, L337 (2001).

[10] R. Movshovich, M. Jaime, J. D. Thompson, C. Petrovic, Z. Fisk, P. G. Pagliuso, and J. L. Sarrao, Phys. Rev. Lett. **86**, 5152 (2001).

[11] J. D. Thompson *et al.*, cond-mat/0012260, J. Magn. Magn. Mater. (to be published).

[12] Yu. N. Grin *et al.*, Kristallografiya **24**, 242 (1979) [Sov. Phys. Crystallogr. **24**, 137 (1979)].

[13] E. G. Moshopoulou, Z. Fisk, J. L. Sarrao, and J. D. Thompson, J. Solid State Chem. **158**, 25 (2001).

[14] K. H. J. Buschow, H. W. de Wijn, and A. M. van Diepen, J. Chem. Phys. **50**, 137 (1969).

[15] N. J. Curro, P. C. Hammel, P. G. Pagliuso, J. L. Sarrao, J. D. Thompson, and Z. Fisk, Phys. Rev. B **62**, R6100 (2000).

[16] A. Benoit, J. X. Boucherle, P. Convert, J. Flouquet, J. Palleau, and J. Schweizer, Solid State Commun. **34**, 293 (1980).

[17] J. M. Lawrence and S. M. Shapiro, Phys. Rev. B **22**, 4379 (1980).

[18] W. Bao, P. G. Pagliuso, J. L. Sarrao, J. D. Thompson, Z. Fisk, J. W. Lynn, and R. W. Erwin, Phys. Rev. B **62**, R14 621 (2000); **63**, 219901(E) (2001).

[19] J. Jensen and A. R. Mackintosh, *Rare Earth Magnetism: Structures and Excitations* (Clarendon Press, Oxford, 1991).

[20] G. L. Squires, *Introduction to the Theory of Thermal Neutron Scattering* (Cambridge University Press, Cambridge, 1978).

[21] M. Blume, A. J. Freeman, and R. E. Watson, J. Chem. Phys. **37**, 1245 (1962).

[22] G. Shirane, Acta Crystallogr. **12**, 282 (1959).

[23] K. Satoh *et al.*, Physica B **186-188**, 658 (1993).

[24] P. G. Pagliuso, J. D. Thompson, M. F. Hundley, and J. L. Sarrao, Phys. Rev. B **62**, 12 266 (2000).